# Supporting Information

# Self-supported layered heterostructure derived from recycling waste silk for high performance low-temperature sodium storage

Zhiwen Long[a], Hao Jia[a,*], Ruizhe Zhang[a], Wei Li[a], Keliang Wang[b,*], Hui Qiao[a,*]

[a] Key Laboratory of Special Protective Textiles, Ministry of Education, College of Textile Science and Engineering, Jiangnan University, Wuxi 214122, China

[b] Institute of Future Technology, Southwest Jiaotong University, Chengdu, Sichuan 610031, China

* Corresponding author. Tel/Fax: +86-510-8591-2009

E-mail: huiqiao@jiangnan.edu.cn (H. Qiao), jiahao@jiangnan.edu.cn (H. Jia), klwang@swjtu.edu.cn (K. Wang)

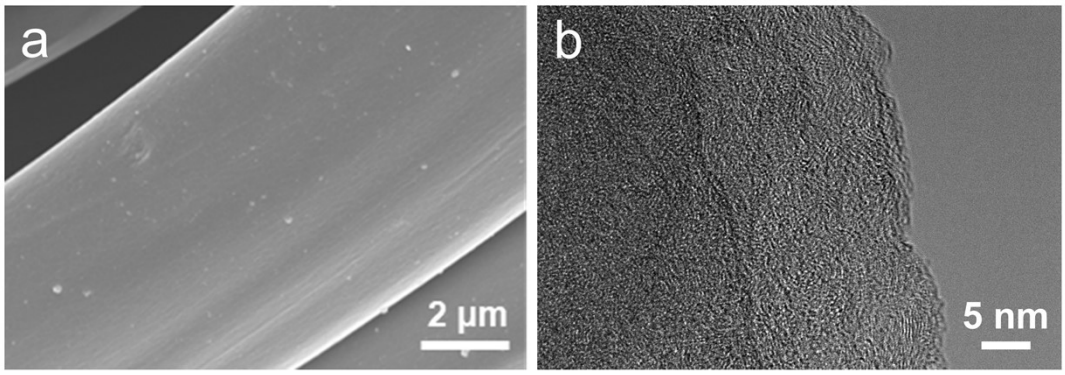


**Fig. S1**. (a) SEM and (b) TEM images of CST

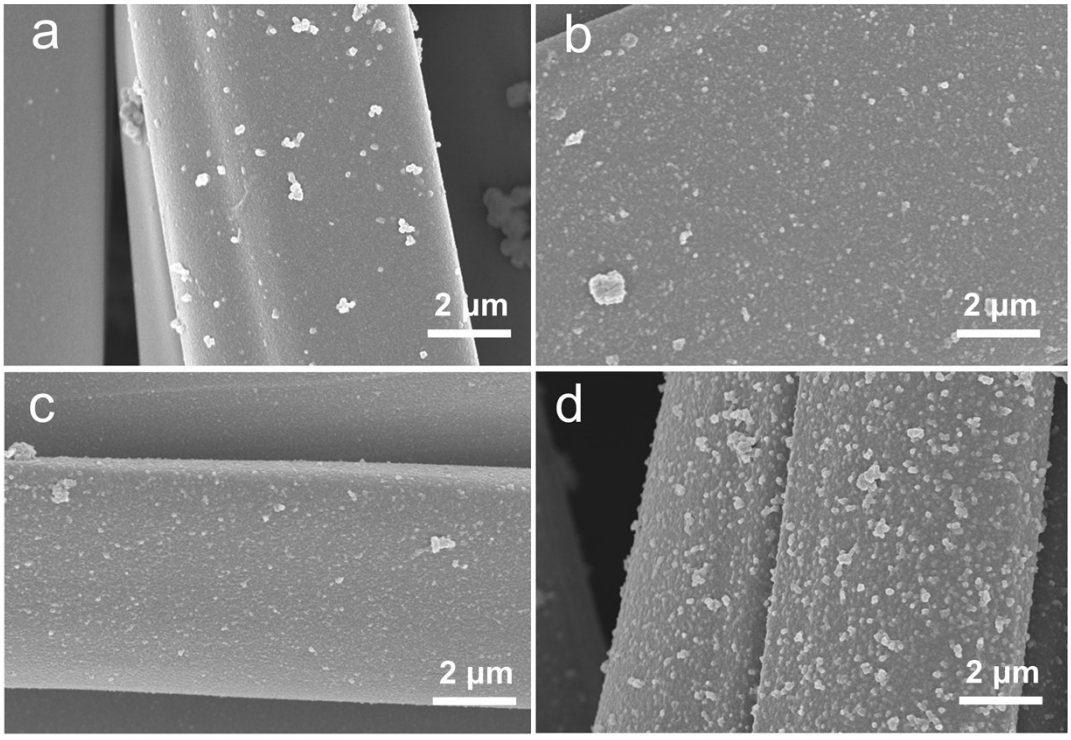


**Fig. S2**. SEM images of (a) $O_2$-assisted PDA coating on CST, (b) $Cu^{2+}$-assisted PDA coating on CST, (c) in-situ growth Sn-Fe-MOF on CST, (d) seed-mediated growth Sn-Fe-MOF on CST

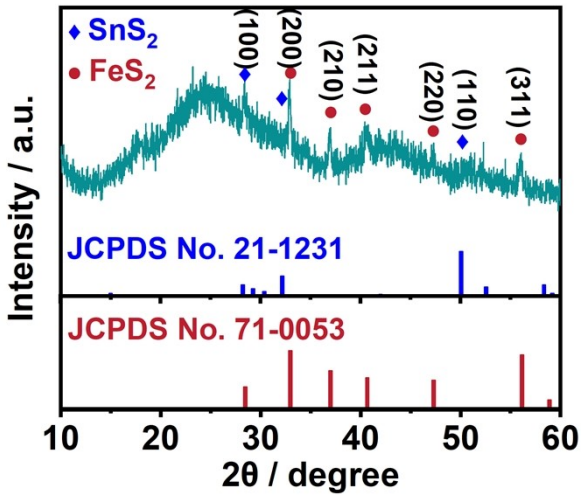


**Fig. S3**. XRD pattern of SFS/CST

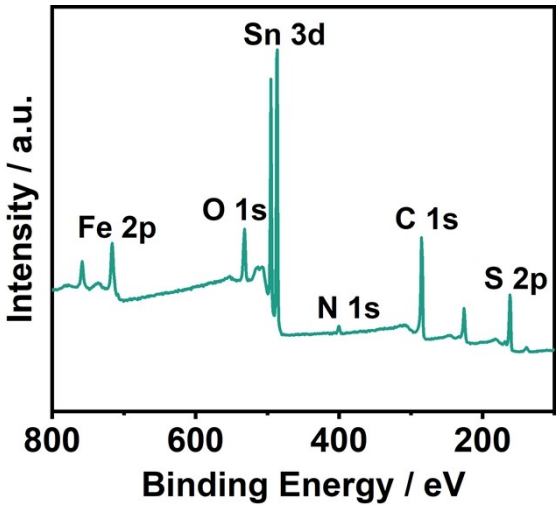


**Fig. S4**. XPS spectra of GO-SFS/CST

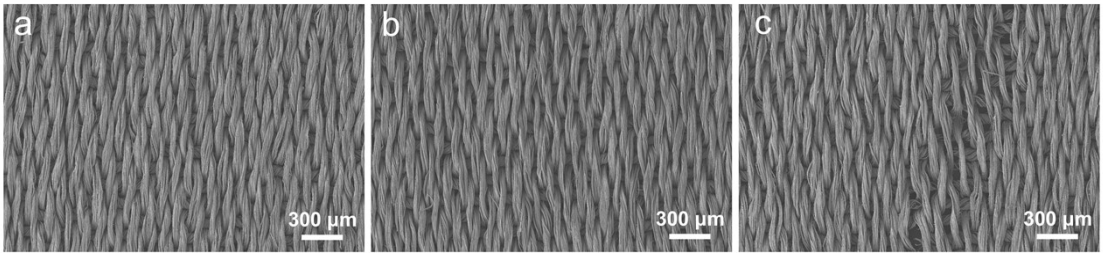


**Fig. S5**. SEM images of GO-SFS/CST (a) before bending cycles, (b) after 500 bending cycles, (c) after 1500 bending cycles

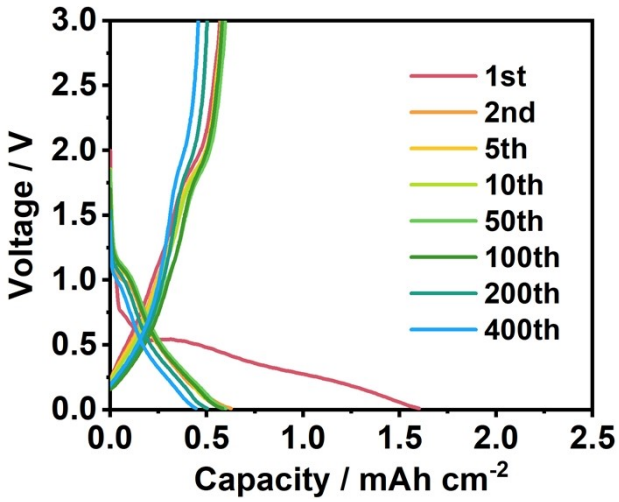


**Fig. S6**. GCD curves of SFS/CST TCEs

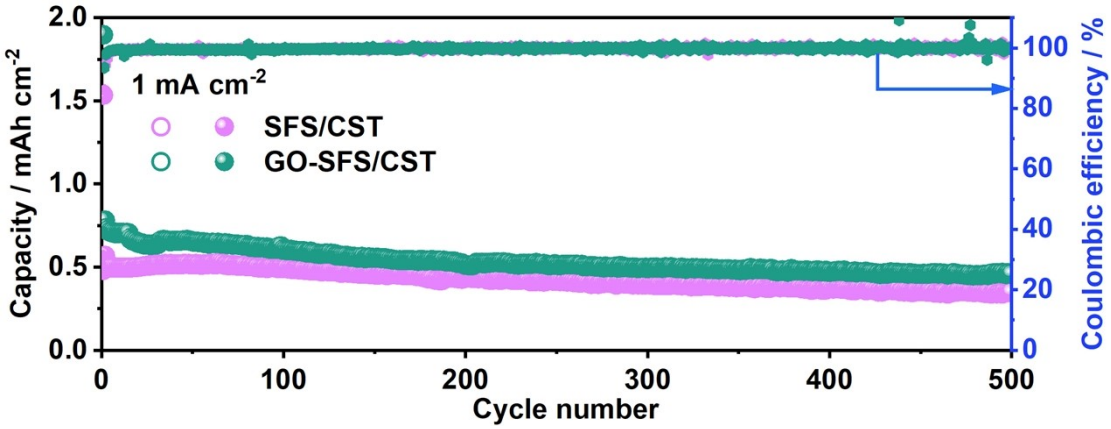


**Fig. S7**. The cycling performance of GO-SFS/CST TCEs and SFS/CST TCEs at current density of 1.0 mA $cm^{-2}$.

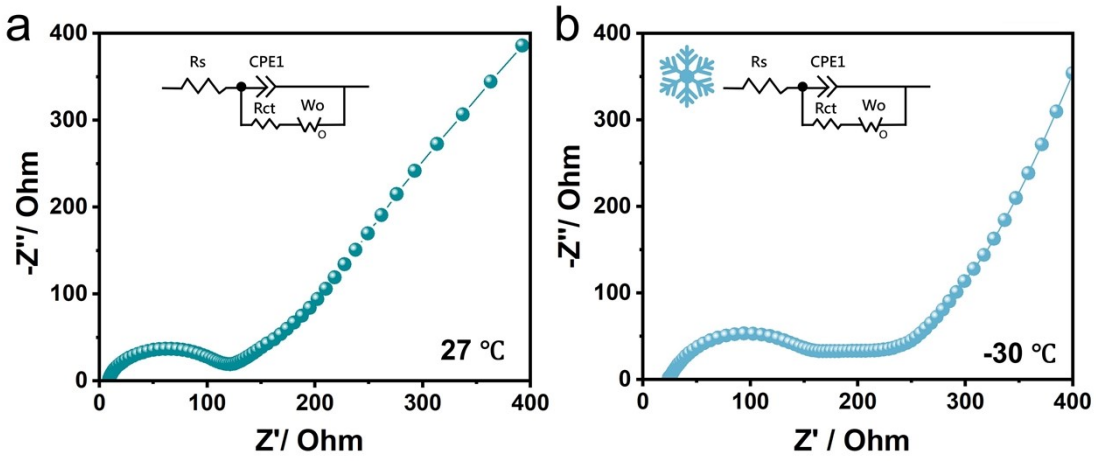


**Fig. S8**. The EIS results of GO-SFS/CST TCEs at 27 and -30 °C after 2 cycles

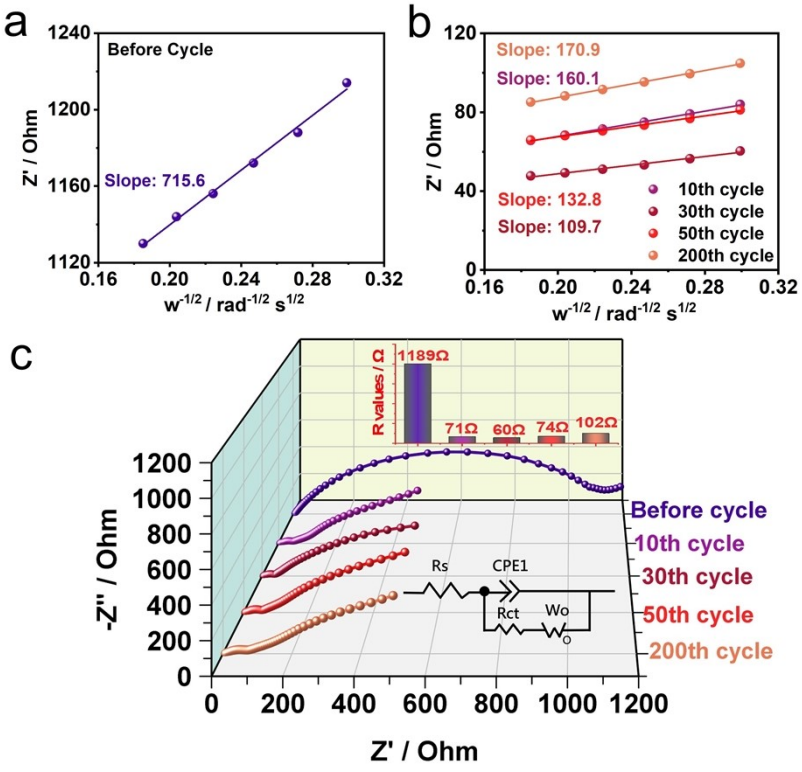


**Fig. S9**. (a) The relationship between Z′ and $\omega^{-1/2}$ and (b) relationship between Z′ and $\omega^{-1/2}$ under different cycle numbers of SFS/CST; (c) The EIS results of SFS/CST TCEs before cycles, after 10 cycles, 30 cycles, 50 cycles and 200 cycles.

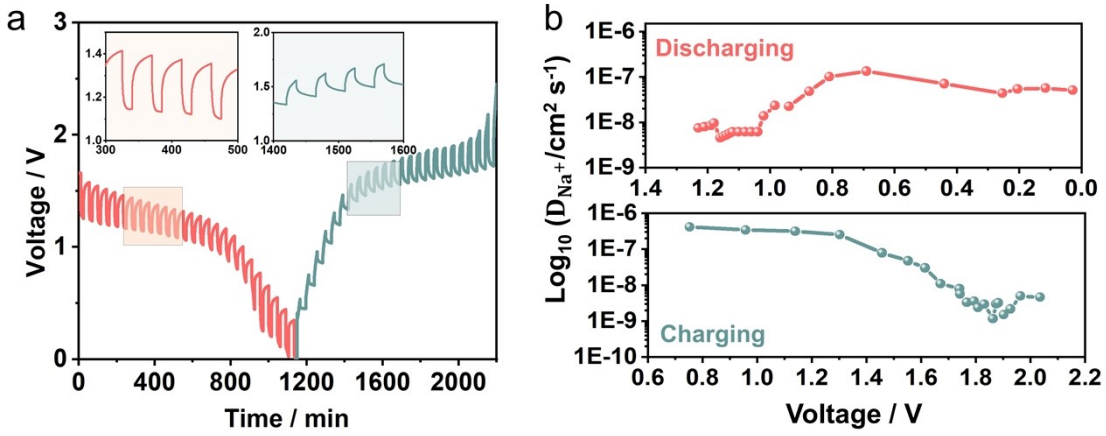


**Fig. S10**. (a) GITT potential profiles and (b) the $Na^+$ diffusion coefficient in charge and discharge of GO-SFS/CST TCEs.

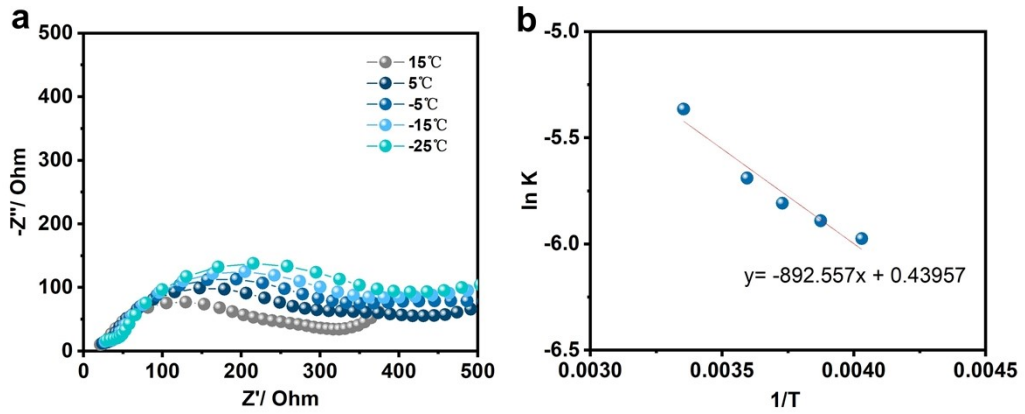


**Fig. S11.** (a) Nyquist plots of GO-SFS/CST at different temperatures ranging from from 15 to -25°C, (b) Arrhenius plot showing the linear relationship between In(1/Rct) and 1/T.

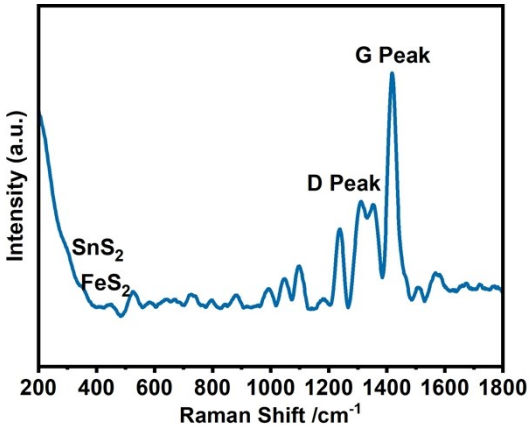


**Fig. S12.** Raman of GO-SFS/CST after 1000 cycles.

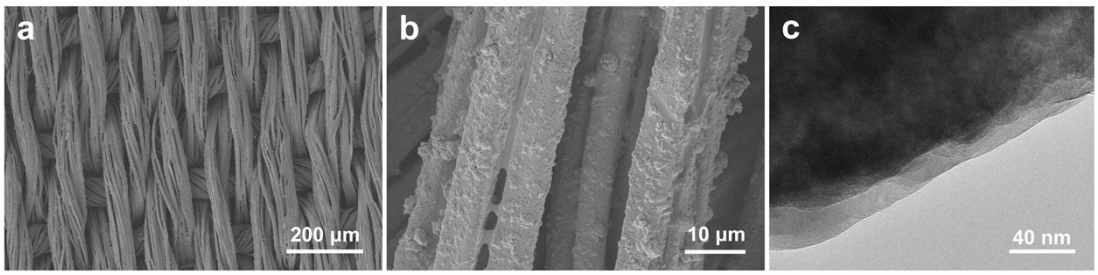


**Fig. S13.** (a, b) SEM and (c) TEM images of GO-SFS/CST TCEs after 500 cycles.

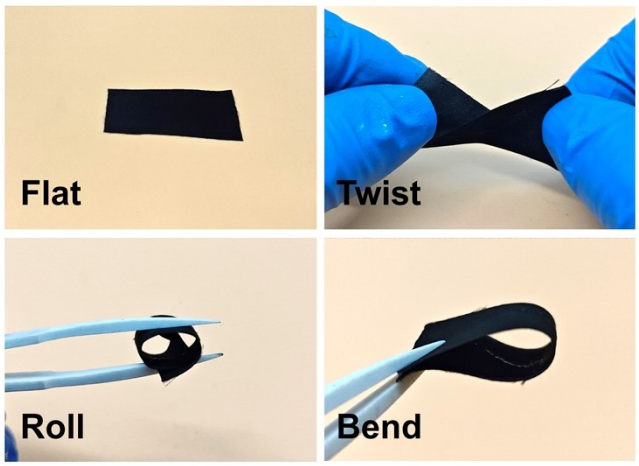


**Fig. S14**. Digital photographs demonstrating the twisting, rolling, and bending deformations of NVP/CST

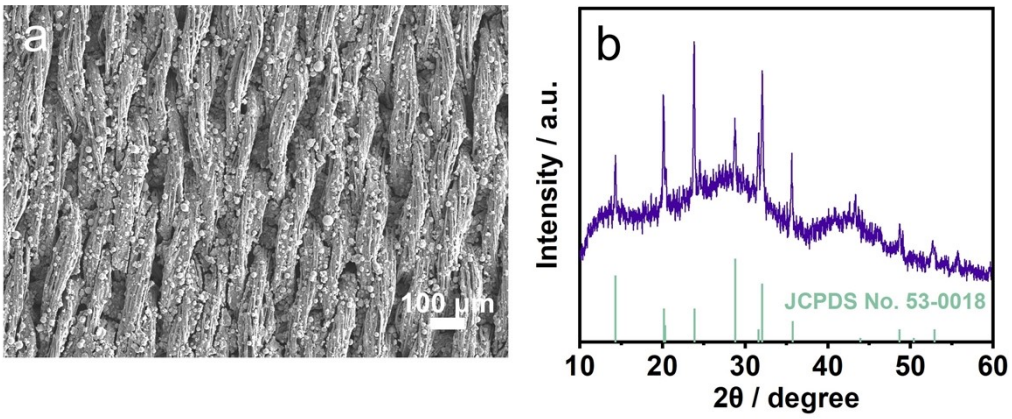


**Fig. S15**. (a) SEM image and (b) XRD pattern of NVP/CST

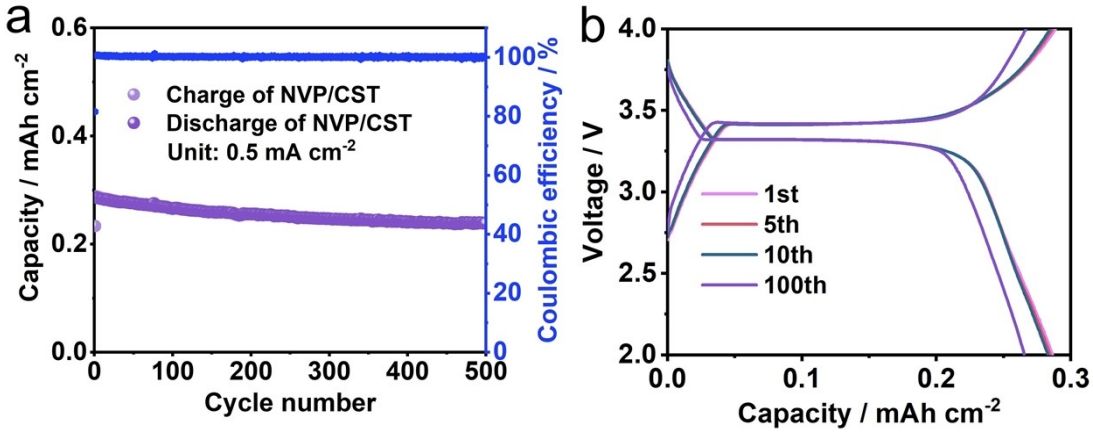


**Fig. S16**. (a) Cycling performance and (b) GCD curves of NVP/CST

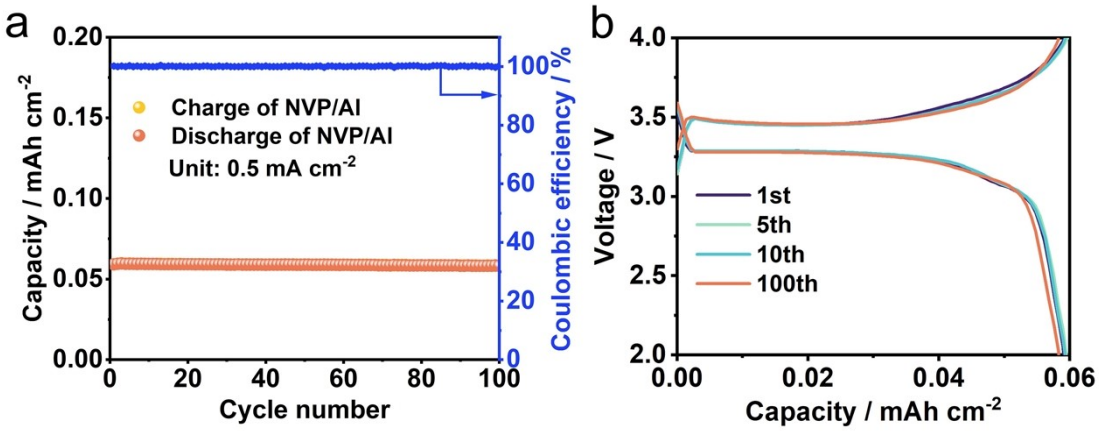


**Fig. S17**. (a) Cycling performance and (b) GCD curves of NVP loaded on the surface of aluminum foil current collectors

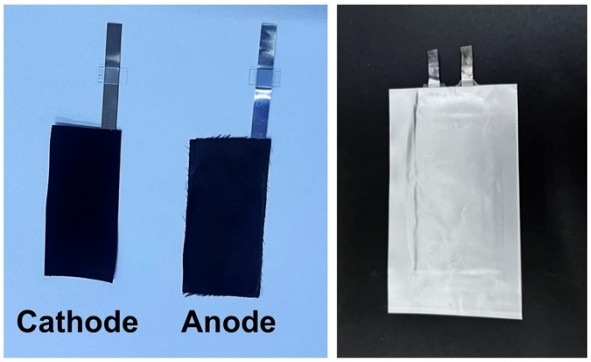


**Fig. S18**. Schematic diagram of the components in a pouch cell battery assembly

**Table S1**. Comparison of electrochemical performance between the GO-SFS/CST and recently reported sulfur-based composite electrodes

| Materials | Current density (A/g) | Capacity (mAh/g) | Cycle Life | Ref |
|---|---|---|---|---|
| $SnS_2/FeS_2$/rGO | 1 A/g | 441.4 mAh/g | 500 | [1] |
| $SnS_2$/rGO/$SnS_2$ | 0.1 A/g | 1133 mAh/g | 100 | [2] |
| $FeS_2$@C@$SnS_2$ | 585.7 mAh/g | 1A/g | 1000 | [3] |
| C@SnS2/SnS@C | 502.5 mAh/g | 2A/g | 1000 | [4] |
| $Bi_2S_3$@NC/$SnS_2$@NC | 290 mAh/g | 5A/g | 1400 | [5] |
| PDC/SnS2@rGO | 295.7 mA h/g | 3A/g | 100 | [6] |
| SnS2@C/CNF | 478.7 mAh/g | 2A/g | 1000 | [7] |
| GO–SFS/CST | 525 mAh/g | 4.37 A/g | 1000 | **This work** |

Reference

[1] Y. Chen, H. Liu, X. Guo, S. Zhu, Y. Zhao, S. Iikubo, T. Ma, Bimetallic sulfide $SnS_2/FeS_2$ nanosheets as high-performance anode materials for sodium-ion batteries, *ACS Appl. Mater. Interfaces* **2021,** *13*, 39248-39256.

[2] Y. Jiang, D. Song, J. Wu, Z. Wang, S. Huang, Y. Xu, Z. Chen, B. Zhao, J. Zhang, Sandwich-like $SnS_2$/Graphene/$SnS_2$ with expanded interlayer distance as high-rate lithium/sodium-ion battery anode materials, *ACS Nano* **2019,** *13*, 9100-9111.

[3] W. Zhao, X. Ma, Y. Zheng, L. Yue, C. Xu, G. Wang, Y. Luo, D. Zheng, S. Sun, A. Ali Alshehri, X. Sun, C. Tang, Hierarchical wormlike engineering: Self-assembled $SnS_2$ nanoflake arrays decorated on hexagonal $FeS_2$@C nano-spindles enables stable and fast sodium storage, *Chem. Eng. J.* **2023,** *459*, 141629.

[4] Y. Tang, F. Wang, C. Nie, H. Dong, Y. Bai, M. Zhao, S. Yang, Rational design of hollow C@$SnS_2$/SnS@C cubes with N-doping to realize stepwise sodium storage induced structural stability for highly stable cycling performance, *J. Power Sources* **2024,** *609*, 234695.

[5] W. Chen, Z. Wang, Z. Huang, W. Xie, J. Zhao, Y. Xiao, S. Lei, B. Huang, B. Cheng, Mixed-dimensional van der Waals heterostructure of $Bi_2S_3$ nanorods and $SnS_2$ nanosheets bridged with N-doped carbon interlayer for enhanced sodium-ion batteries, *Energy Storage Mater.* **2024,** *73*, 103880.

[6] Y. Sun, Y. L. Yang, X. L. Shi, L. Ye, Y. Hou, J. Wang, G. Suo, S. Lu, Z. G. Chen, An ultra-stable sodium half/full battery based on a unique micro-channel pine-derived carbon/$SnS_2$@reduced graphene oxide film, *Battery Energy* **2023,** *2*, 20220046.

[7] Z. Cui, S. A He, J. Zhu, M. Gao, H. Wang, H. Zhang, R. Zou, Tailoring the void space using nanoreactors on carbon fibers to confine $SnS_2$ nanosheets for ultrastable lithium/sodium-ion batteries, *Small Methods* **2022**, *6*, 2101484.